International Refereed Journal of Engineering and Science (IRJES)
ISSN (Online) 2319-183X, (Print) 2319-1821
Volume 13, Issue 6 (Nov.-Dec. 2024), PP. 18-29

Removal of Aluminum (Al^{+3}) and Copper (Cu^{+2}) from a Chemical Industry Wastewater with Graphene Oxide (GO) / Zinc Oxide (ZnO) Nanocomposite

Sevil AKÇAĞLAR
Department of Mechanical Engineering, Faculty of Engineering, Dokuz Eylül University, İzmir, Turkey, Corresponding Author: sevil.akcaglar@deu.edu.tr

Abstract: *In order to remove the Al^{+3} and Cu^{+2} metals from an chemical industry wastewaters adsorption technology was used with a nanocomposite namely graphene oxide (GO)/ zinc oxide (ZnO) nanocomposite produced under laboratory conditions. The functionalization of GO with zinc oxide nanoparticles (ZnO) improved the adsorption capacity of aluminum (Al^{+3}) and copper (Cu^{+2}). FT-IR spectra of GO, ZnO and GO/ZnO exhibited maximum absorption bands at 3401 1/cm 1842 1/cm and 1197 1/ cm corresponding to the stretching OH-groups and C=O bonds. The GO doped with ZnO nanoparticles exhibited good performances compared to both separete ones. The surface area, pore volume, pore diameter and adsorption capacity of the produced nanocomposite were 54.22 m^2/g, 0.45 cm^3/g, 32.09 nm and 0.54 mmol/g,respectively. For maximum adsorption efficiencies of Al^{+3} and Cu^{+2} (99% and 96%), GO/ZnO nanocomposite concentration, Ph, and temperature should be 40 mg/l, 6.00, and 25 ^oC, respectively. Cu concentrations are limited to 120 minutes and 400 mg/l. The adsorption was generated according to Langmuir adsorption isoterm and kinetic constants were relevant with second pseudo order reaction kinetic. The KL and qL for Al adsorption were 0.79 l/mg and 47 mg/mg while the same parameters were 0.70 l / mg and 44 mg/mg for Cu adsorption.*
Keywords*: Adsorption, Chemical industry,; Graphene oxide, Zinc oxide, Nanocomposite, Al, Cu*

Date of Submission: 06-11-2024 Date of acceptance: 18-11-2024

I. INTRODUCTION

High metals concentrations are toxic to both humans and the living organisms in aquatic ecosystems. Metals come from volcanic activities and anthropogenicactivities provides environmental problems derived from chemical industry wastes [1]. Many rivers have high concentrations of heavy metals, which limits the potential uses of water [2,3]. Thus, new treatment processes are necessary to ameliorate the polluted water. The chemical industry comprises the companies that produce industrial chemicals. Chemical industrial wastewaters usually contain organic and inorganic pollutants at elevated concentrations. Many materials in the chemical industry are toxic, carcinogenic and are inert. It can not be removed biologically. For instance, Al and Cu producing chemical products can not be treated effectively with conventional treatment processes. However, regulations that govern the allowable discharge of Cu^{+2} and Al^{+3} into sewage treatment plants and surface water bodies are becoming increasingly stringent [4,5].

It is important to mention that aluminium is toxicologically important for environmental point of view and Alzheimer's disease is a symptom of chronic aluminium intoxication over decades or breast cancer. Copper (Cu^{+2}) is an essential element for humans and plants when present at low concentration, while in excessive amounts it exerts detrimental effects. Therefore, a detrimental effect can be detected at all organisms in environment at high concentration of Cu^{+2} [6,7].

Conventional treatment processes to remove the metals from wastewater were coagulation/flocculation, precipitation, ion exchange, and membrane filtration [8]. Adsorption process exhibited main advantages with high removal efficiency, regeneration properties and reduced cost process of the adsorbents [9]. The adsorbents, such as zeolites, activated carbons, biochars and biomaterials can be used to remove the metals however low removal yields was detected. Nanomaterials have come to the forefront mainly due to their high specific surface area, which is known as one of the main factors determining adsorption magnitude [11,12].

Graphene oxide (GO) has been considered especially as a nano-adsorbent for heavy metals. Along with its large surface area and the abundant presence of oxygen-containing functional groups, is the main reasons for

its high efficiency for adsorbing of metals [13,14]. Thus, GO can adsorb some metals like cobalt (Co), cadmium (Cd), copper (Cu), iron (Fe), nickel (Ni), lead (Pb) and strontium (Sr) [15].

In order to improve the adsorption capacity of GO carboxylation (GO-COOH) process was carried out. This increased the Cu and Co adsorptions [16]. Graphene oxide was doped with zinc oxide nanoparticles (GO/ZnO) and effectively used in adsorptions of Cu, Cd, Co, Cr, Hg and Pb metals [17]. Zinc oxide (ZnO) nanomaterials have been shown to adsorb Cu, Cd, Mn, Pb and Hg. Since ZnO nanoparticles are small and unstable, it is very important their binding into porous supports to provide larger adsorbents [18]. Although GO and GO/ZnO nanocomposites have been reported as efficient metal adsorbents, no studies was found about the removals of Al and Cu from a chemical industry wastewaters.

Therofore, in this study it was aimed to remove the Al^{+3} and Cu^{+2} metals from a chemical industry wastewater using GO/ZnO nanocomposite. The physicochemical properties of properties of the GO/ZnO nanocomposite was investigated with FT-IR and SEM-EDX analysis. The adsorption of GO/ZnO nanocomposite was characterized using Langmuir and Freundlich model isotherms. The effects of some operational conditions (GO/ZnO nanocomposite, Al and Cu concentration, adsorption time and pH) on Cu^{+2} and Al^{+3} adsorption yields were detected.

II. MATERIALS AND METHODS

2.1. Preparation of GO

GO was prepared with 31 mg/l $KMnO_4$, 400 ml H_2SO_4 , 10 g graphite powder and with 5 g $NaNO_3$. This mixture was cooled using an ice bath to 0 °C. The reaction was warmed at 35 °C and stirred for 8 h. The mixture was cooled and was mixed with 500 ml of 40% H_2O_2 .The mixture was washed in a 15% HCl solution; and was filtered using a 0.55 µm membrane filter. The filtrate was centrifuged and the supernatant was decanted. The solid settled was cleaned by distilled water for 9 days to remove the residual materials. The suspension was diluted at a ratio of 1 to 3 and during 14 hours. The resulting solution was died at an oven at 80 °C for 5 h.

2.2. Preparation of GO/ZnO nanocomposite

Commercial ZnO nanoparticles ere used for the preparation of GO/ZnO nanocomposites. ZnO nanoparticles were dispersed into 10 ml ethanol, and the solution was sonicated for 50 min. Then, 400 mL of ZnO solution was mixed with 180 mL of GO. The mixture was evaporated for ethanol removal. The GO/ZnO nanocomposite was obtained after maintaned in at 80 °C for 5 h.

2.3. Characterization GO/ZnO nanocomposites

GO, ZnO and GO/ZnO, were characterizate with Fourier transform infrared (FT-IR) spectra (KBr pellet method, 400–4000 1/cm) on a FT-IR 4600 Spectrometer (USA). The specific surface areas of the samples were determined by Brunauer–Emmet–Teller analysis (BET) N_2 adsorption–desorption analysis (USA). The surface morphology was determined by using a scanning electron microscope (SEM) (Japan) coupled with energy-dispersive X-ray spectroscopy (UK).

2.4. Adsorption studies

Batch experiments were conducted to obtain the isotherms for Al^{+3} and Cu^{+2} for GO and GO/ZnO nanocomposites. Experiments were carried out at increasing concentrations of Al^{+3} (40.0 mg/L–500 mg/L) and Cu^{+2} (40–500 mg/L). The experiments were performed in a glass reactor at increasing pH values (4, 6, 10). Batch experiments were performed with shaking at 22 °C for 20 h. After equilibrium, aqueous phases were separated from the solids by centrifugation filtered through 0.35 µm membranes to measure the residual Al^{+3} and Cu^{+2} concentrations. The sorption capacity qe (mg/g nanocomposite) was calculated using Equation (1):

$$qe=(C_0-Ce)\times Vm \quad \text{qe=(C}_0\text{−Ce)×Vm} \qquad (1)$$

where C_0 is the initial concentration (mg/L), Ce is the aqueous-phase equilibrium metal concentration (mg/L), V is the volume of wastewater (L), and m is the mass of the nanocomposite (g).

2.5. Adsorption Isotherms

The experimental data obtained from the adsorption experiments were fitted using Langmuir and Freundlich models. The sorption capacity q (mg/g sorbent) for Langmuir, Freundlich, Tempkin and Dubinin–Radushkevich models was obtained using Equations (2)–(5), respectively.

$$q = \frac{qL\ Kl\ Ce}{1+KL\ Ce} \quad (2)$$

$$q = KF\ (Ce)1/n \quad (3)$$

$$q = B\ \ln\ At\ Ce \quad (4)$$

$$q = qs\ \exp\ (-\ kad\ \boldsymbol{\varepsilon}^2\ ) \quad (5)$$

where
-qL: amount of adsorption corresponding to a monolayer coverage;
-KL: Langmuir constant related to the energy of adsorption;
-KF: constant related to adsorption capacity;
-n: constant related to adsorption intensity;
-At: Tempkin isotherm equilibrium binding constant (L/g);
-B: short form of expression RT/b_t, where R, T and b_t represent the gas constant (8.314 J/mol K), absolute temperature (K) and Tempkin isotherm constant;
-qs: theoretical isotherm saturation capacity (mg/g);
-kad: Dubinin–Radushkevich isotherm constant (mol^2/kJ^2);
-ε: Short form of expression can be defined as follows:

$$RT\ \ln\ [1 + \frac{1}{Ce}]$$

where R and T represent the gas constant (8.314 J/mol) and absolute temperature (K);
-Ce: equilibrium concentration of metal in aqueous solution (mg/L)

2.6. Kinetic Studies

In the kinetic studies, 30 mg of each adsorbent was added to 60 mL of chemical industry wastewater. The samples were taken at 30 min, 1 h and 22 h. The kinetic experimental data were fitted using a pseudo-first order and pseudo-second-order kinetic equations. The pseudo-first-order (6) and the pseudo-second-order (7) are showed as follows:

$$\log\ (qe - qt) = \log\ qe - \frac{k_1}{2.303}\ t \quad (6)$$

$$\frac{t}{qt} = \frac{1}{k_2 qe^2} + \frac{1}{qe} \quad (7)$$

where
-qeqe: adsorption capacity at equilibrium (mg/g);
-qtqt: adsorption capacity at the time t (mg/g);
-$k1$k1: constant of first-order adsorption (1/min);
-$k2$k2: constant of second-order adsorption (g/(mg·min).

In order to characterize the kinetic curve of the pseudo-second-order model, the approaching equilibrium factor (R_w) was determined (Equation 8):

$$R_W = \frac{1}{1+k_2\ qe\ tref} \quad (8)$$

where $tref$: longest operation time (based on kinetic experiments)

2.7. Al and Cu analysis

Al and Cu concentrations were measured using a UV-vis spectrophotometer (DR3900, Hach, USA) according to Standard Methods (2020) [18].

III. RESULTS AND DISCUSSION

3.1. GO/ZnO Nanocomposite Characterization

3.1.1. FT-IR Analyses Results

FT-IR analyses were performed to investigate the chemical structure of nanoparticles. FT-IR spectra of GO, ZnO and GO/ZnO exhibited that GO has an absorption band at 3401 1/cm which corresponds to the stretching OH-groups vibrations. This showed the presence of hydroxyl groups in the GO (Figure 1). The maximal absorption peaks at 1842 cm^{-1} and 1197 1 /cm correspond to the C=O stretching [19]. The carbonyl signal can be related to carboxylic acids, and aldehydes. The absorption peak at 1485 cm^{-1} exhibited the C-H groups. The maximal disturbances at 1299 1/cm and 1109 1/cm are relevant to the C-O stretching [20].The characteristic signals of ZnO was detected around 800 cm^{-1}, which corresponds to the IR spectra [21]. The FT-IR spectrum for GO/ZnO exhibited stretching vibration of the O-H groups illustrated at 3402 cm^{-1} was defined with the bonds contains oxygen. The special signals of ZnO are showed at 783 cm^{-1} and 466 cm^{-1}.

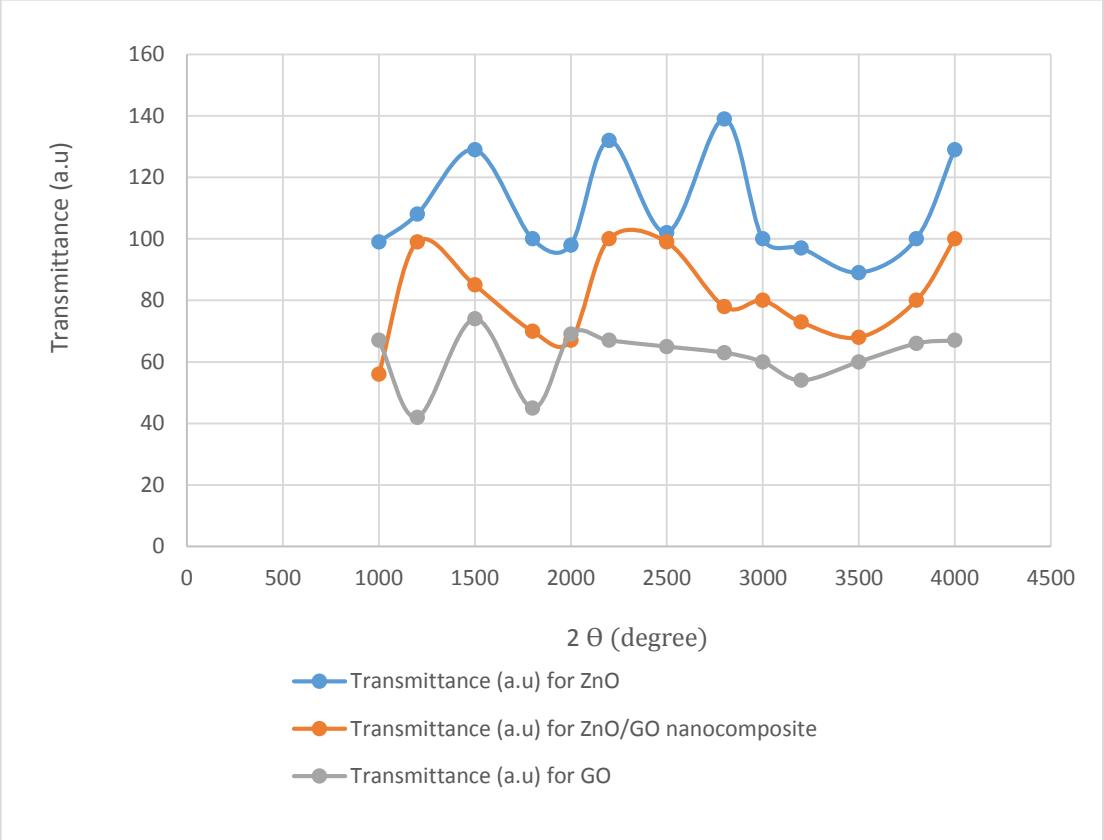

Fig. 1. FT-IR spectrum of GO, ZnO and GO/ZnO nanoparticles

3.1.2. BET Analysis Results

BET was employed to compare the surface properties of GO, ZnO and GO/ZnO nanoparticles. The ZnO nanoparticles showed higher values for BET surface area (48.77 m^2 / g), pore volume (0.43 cm^3 / g), pore diameter (32.99 nm) and sorption capacity (0.49 mmol / g) than GO (26.14 m^2 / g, 0.09 cm^3 / g, 17.06 nm and 0.24 mmol / g, respectively). These results can be explained due to smaller size of the ZnO nanoparticles (< 30 nm) and their good dispersibility in water [22]. However, the GO doped with ZnO nanoparticles exhibited good performances compared to both separete ones. The surface area: 54.22 m^2/g; pore volume: 0.45 cm^3/g; pore diameter: 32.09 nm; and sorption capacity: 0.54 mmol/g (Table 1).

Table 1.BETanalysis results of GO, ZnO and GO/ZnO nanoparticles

Properties	Nanocomposites		
	GO	ZnO	GO/ZnO
BET surface area (m^2/g)	22.45	48.77	52.22
pore volume cm^3/g	0.33	0.43	0.45
pore diameter (nm)	29.97	32.99	32.09
sorption capacity (mmol/g)	0.43	0.49	0.54

3.1.2. SEM analysis results

The SEM results of GO, ZnO and GO/ZnO are illustrated in Figure 2a, b and c. GO has a layered structure and is mainly composed of carbon and oxygen. Figure 2d exhibited the ZnO nanoparticles generating some agglomerations. These nanoparticles are mainly composed of zinc and oxygen, and carbon [23].

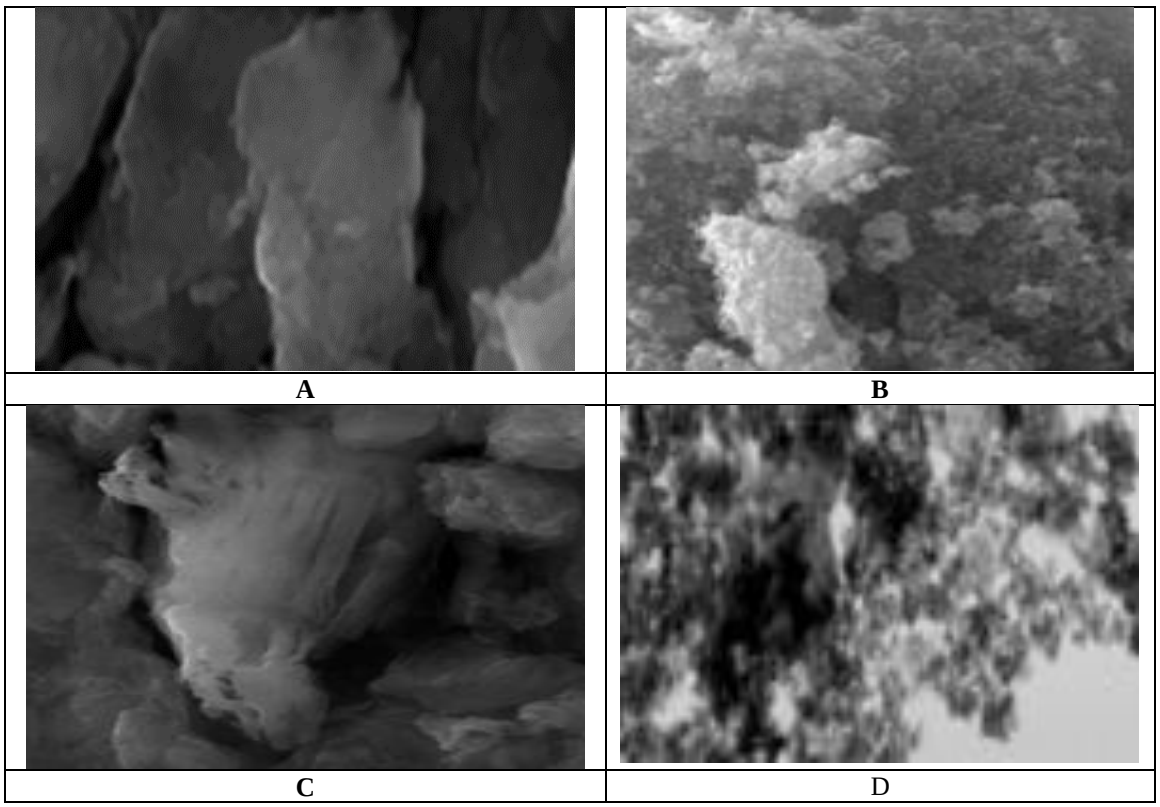

Fig. 2. (a) SEM images of GO, (b) ZnO, (c) GO/ZnO nanocomposite and (d) Agglomeration of ZnO in the GO/ZnO nanocomposite

3.1.3. XRD analysis results

XRD patterns of the pure ZnO, GO and GO-ZnO composite are shown in Figure 3. The XRD pattern of GO showed an intense diffraction peak at $2\Theta = 11.6°$, which is related to the (001) lattice plane structure of GO. The major peaks of ZnO were observed in XRD pattern of pure sample and showed a maximum disturbance (102) at (~38.30°) of ZnO structure. ZnO peaks matched well with the standard data for wurtzite structure of ZnO (JCPDS card no. 36–1452 data) [24].

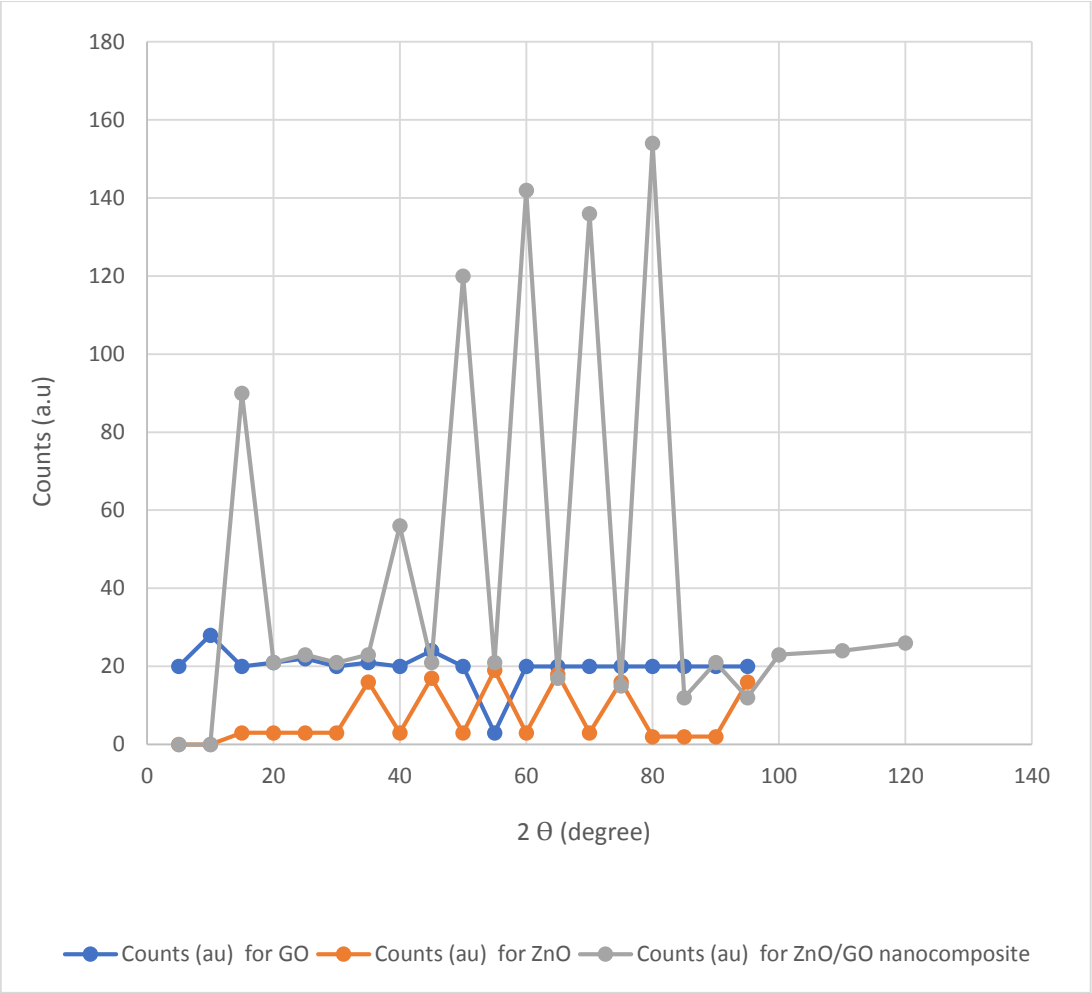

Fig. 3. XRD pathways of ZnO, GO and GO-ZnO composite

3.1.4. EDX analysis results

EDX analysis shows the presence of zinc and doped to GO. The main constituent elements are carbon and oxygen while a part of the ZnO was shown in the structure of ZnO/ GO nanocomposite (Table 2).

Table 2. Ingredients of GO, ZnO and ZnO/ GO nanocomposite

Compound name	EDX (C) Weigth %	EDX (O) Weigth %	(EDX Zn) Weigth %
GO	55, 3	44, 2	-
ZnO	45	33	4, 29
ZnO/ GO	57	39	3, 4

The SEM-EDX results show the compositions for zinc oxide-graphene nanocomposites, where the elemental composition percentage follows the order C > O > Zn.

3.1.5. Raman Spectra results

For study the bonding environment and defect related disorder in ZnO and GO-ZnO composite, Raman analysis was performed. ZnO with wurtzite symmetry structure belongs to the C6V 4 space group (P63mc) [25]. (Fig. 4) [25]. For ZnO, there are active modes including an A1 branch, two doubly degenerate E2 branches, a doubly degenerate E1 branch and also inactive modes as two B branches. Generally, in Raman study, most of ZnO peaks were observed at 332, 386, 437, 543, 583, 660, 990 cm^{-1}. As shown in Figure 4, the Raman spectra for the ZnO nanopowder showed a strong peak at ~437 cm^{-1} that is corresponded to the E2 mode. Also another

peak around 332 cm^{-1} was observed which is a second-order structure of ZnO resulted from transverse optical photons [26].

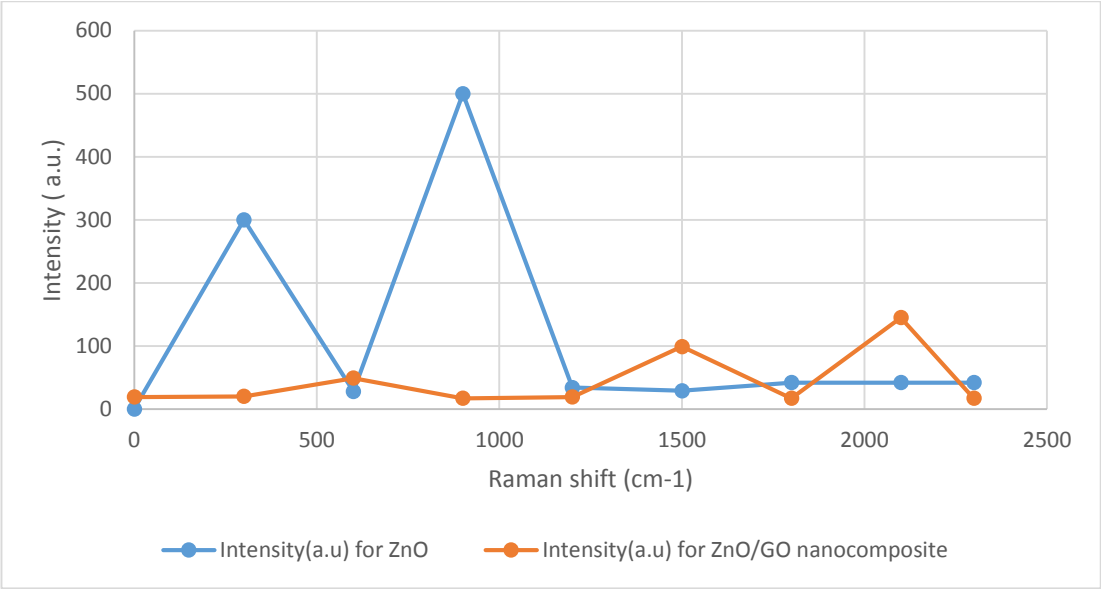

Fig. 4. Raman spectra of ZnO and GO-ZnO composite

3.2. Adsorption Experiments

3.2.1 Effect of pH

The pH_{PZC} is an important parameter that indicates the pH value at which the surface is neutral. This implies that at a pH higher than this point, the surface is negatively charged, so it has an affinity for positive charges for metal adsorption. The determination of pH_{PZC} for GO was performed and it was found between 3.2 and 3.8 (data not shown). For GO/ZnO nanocomposites, pH_{PZC} is 6.0 (data not shown).

The Ph of the chemical industry wastewaters was found to be 5.95. Both pH values are higher than the GO pH_{PZC} but are below than the GO/ZnO pH_{PZC}. This condition should favor GO more than the GO/ZnO in the affinity for metal ions, according to the surface charge of the nanoadsorbents under these pH values. Table 3 indicates the effect of Ph on removals of Al and Cu. The maximum yields for both metal was found at pH=6.0.

Table 3. Effect of pH on adsorption yields of Al and Cu

Ph values	Al adsorption yields (%)	Cu adsorption yields (%)
4	67	64
6	99	98
10	60	55

3.2.2. Effect of adsorption Time

Increasing of adsorption times (40, 80, 120 and 150 min) on the removals of 300 mg/l of Al and 200 mg/l Cu was investigated at pH=6.0 and at a temperature of 25ºC, respectively (Table 4). 45.14%- 56%, 62.28%-79%, 99.17%-96 % and 86.89%-83% removal yields were obtained after 20 min, 40 min, 80 min and 150 min, respectively, for Al and Cu (Table 4). The maximum 99.17% removal efficiency was observed after 120 min photodegradation time for Al while the recorded Cu removal was 96%(Table 4).Further increase of time to 150 min sligtly reduced both yields.

Table 4. Effect of adsorption time on the yields of Al and Cu

Adsorption time (min)	Al adsorption yields (%)	Cu adsorption yields (%)
40	56	45.14
80	79	62.28
120	99.17	96
150	86.99	83

3.2.3. Effect of increasing ZnO/GO nanocomposite concentrations on the yields of Al and Cu

Increasing of nanocomposite concentrations (10, 20, 40, 80 and 100 mg/l) on the adsorption yields of Al and Cu were examined after 120 min photodegradation time, at pH=6.0, at 25ºC (Table 5). 24.43%-21.00%, 49.65%-40.76%, 99.12%-96.22% and 88.04%-78.34% removal yields were measured at 10 mg/l, 20 mg/l, 40 mg/l and 100 mg/l ZnO/GO concentrations, respectively, for Al and Cu adsorption after 120 min photodegradation time, at pH=6.0, at at 25ºC, respectively (Table 5). The maximum adsorption yields for Al and Cu were 99.12% and 96.22%,respectively at 40 mg/l ZnO/GO concentration .

Table 5. Effect of increasing ZnO/GO nanocomposite concentrations on the yields of Al and Cu

ZnO/GO nanocomposite concentration (mg/l)	Al adsorption yields (%)	Cu adsorption yields (%)
10	24.23	21.00
20	49.65	40.76
40	99.17	96.22
100	88.04	78.34

3.2.4. Effect of increasing Al and Cu concentrations on the yields of Al and Cu

The effect of increasing Al and Cu concentrations (50, 150, 200 , 300, 400, 600 mg/l) on the adsorption yields of Al and Cu were studied after 120 min photodegradation time, at pH=6.0, at 25ºC (Table 6). 99%-96%, 99%-96%, 99%-96%, 99%-96% and 89.99%-80.76% removal yields were measured at 10 mg/l, 20 mg/l, 40 mg/l and 100 mg/l ZnO/GO concentrations, respectively, for Al and Cu adsorption after 120 min photodegradation time, at pH=6.0, at at 25ºC, respectively (Table 6). The maximum adsorption yields for Al and Cu were 99% and 96%,respectively up to Al and Cu concentration of 600 mg/l . At 600 mg/l Al and Cu concentrations the Al and Cu adsorption yields decreased to 89.99% and 80.76%, respectively.

Table 6. Effect of increasing Al and Cu concentrations concentrations on the yields of Al and Cu

Individual Al and Cu concentrations (mg/l)	Al adsorption yields (%)	Cu adsorption yields (%)
50	99	96
150	99	96
200	99	96
300	99	96
400	99	96
600	89.99	80.76

3.2. Adsorption isotems

Adsorption experimental data were fitted using Langmuir, Freundlich and Tempkin and Dubinin–Radushkevich isotherm models. According to the statistical analysis of all the experimental conditions and calculatedkinetic constants, the results presented a better fit using the Langmuir model. This model is characterized by assuming a monolayer adsorption, on the surface of ZnO/GO resulting finite number of sites for bonding of Al and Cu (Table 7) [27].

Table 7. Adsorption studies with Langmuir, Freundlich, Tempkin and Dubinin–Radushkevich isotherm models

	Langmuir			Freundlich		Tempkin		Dubinin-Radushkevich				
	For Al adsorption											
Nanomaterials	$_L$	$_L$	^{2}	$_F$		^{2}	$_T$		^{2}		$_{ad}$	^{2}
GO	6	.12	.99	.88	.42	.90	88	.67	.80	4	.002	.79
ZnO/GO	7	.79	.99	.94	.34	.90	29	1.04	.80	4	.004	.70
	For Cu adsorption											
GO	9	.10	.99	.67	.99	.90	45	.45	.75	9	.001	.69
ZnO/GO	4	.70	.99	.78	.30	.90	99	.67	.75	8	.003	.65

Where the units were as follows:

$q_{L\ (mg/mg)}$, $K_{L\ (l/mg)}$, $K_{F\ (l/g)}$, $A_{T(l/g)}$, $q_{(mg/g)\ and}$ $k_{ad\ (mol^2/Kj^2)}$

3.3.1. Langmuir fits for Al and Cu Adsorptions

Experimental results for Langmuir fit are shown in Figure_5 for Al (a) and Cu (b) . The GO/ZnO reached a higher maximum sorption capacity for the removal of Al and Cu, with values of 47 and 44 mg/g, respectively, compared to the results obtained using only GO nanoparticles at pH= 6 after 120 min adsorption at 400 mg/l Al and Cu concentration at 40 mg/l nanocomposite concentration.

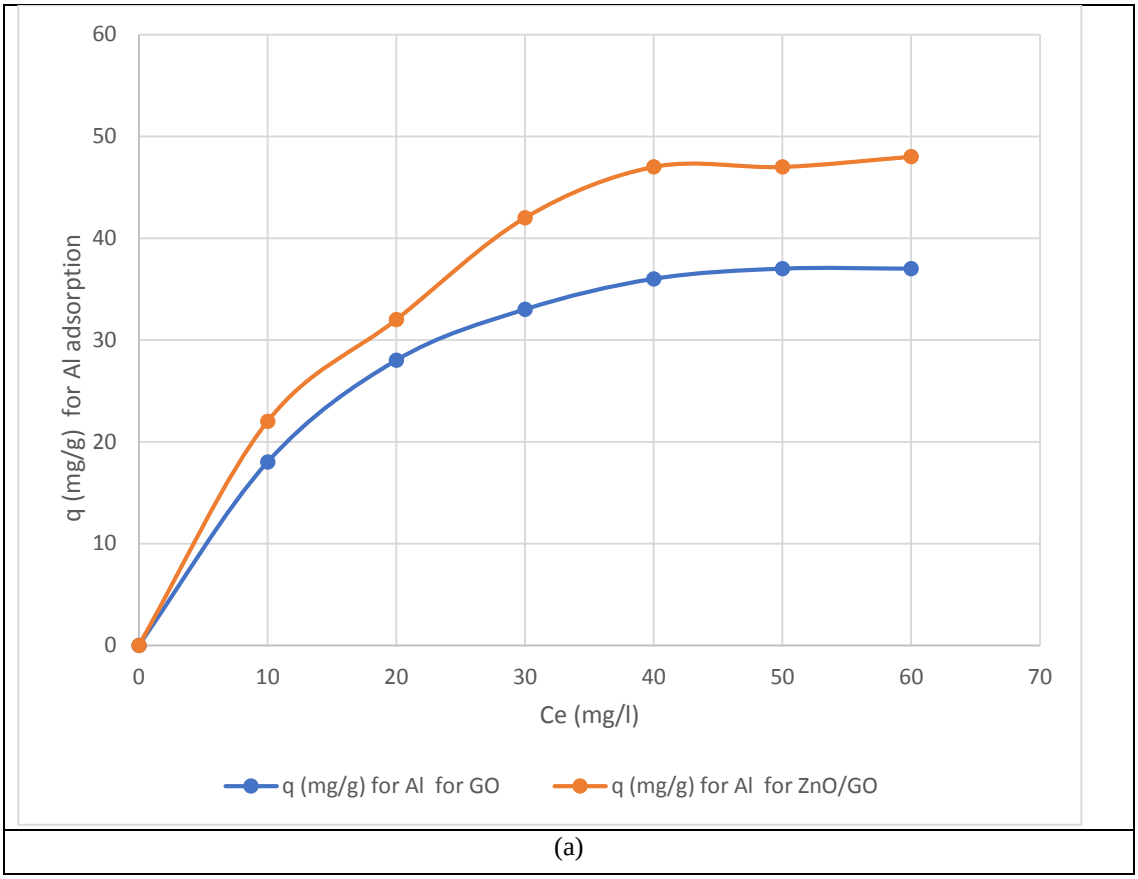

(a)

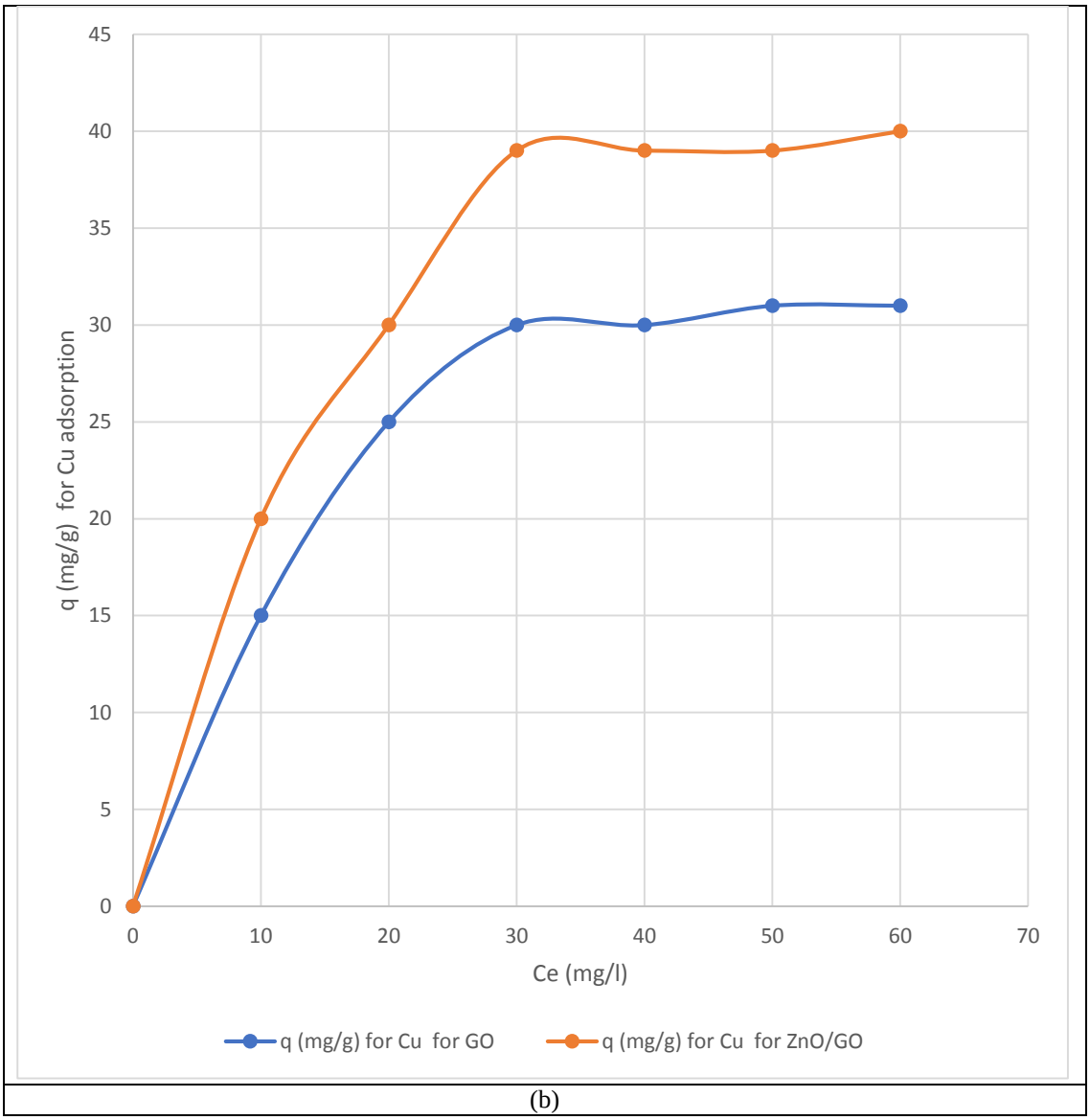

(b)

Fig. 5. Adsorption isotherms for (a) Al and (b) Cu during adsorption experiments with GO and ZnO/GO nanocomposite

3.2.2. Kinetic studies

Experimental data obtained from the adsorption studies were fitted with pseudo-first-order and pseudo-second-order kinetic models. The kinetic adsorption parameters for both models are shown in Table 8. According to the values of the coefficient of determination (R^2) and the theoretical adsorption capacities associated with each model (q_{e1} and q_{e2}), it was determined that the model that presents a better fit is the pseudo-second-order. The kinetic curves are presented in Figure 6. These fits showed that the adsorption capacity of Al and Cu on ZnO/GO nanocomposite was observed as a function of time[27 28].

The pseudo-second order kinetic model was found to be the most used fit for the adsorption of metal ions.

Table 8. Compairison of pseudo-first-order and pseudo-second-order kinetic models for Al and Cu adsorption

	Experimental q (mg/g)	Pseudo first order			Pseudo second order		
		k_1 (1/min)	q_e 1(mg/g)	R_2	k_2(g/mg.min)	q_e 2(mg/g)	R_2
For 50 mg/l initial Al concentration	45	0.0008	291	0.78	0.0028	36	0.99
For 49 mg/l initial Cuconcentration	40	0.0006	321	0.73	0.0022	30	0.99

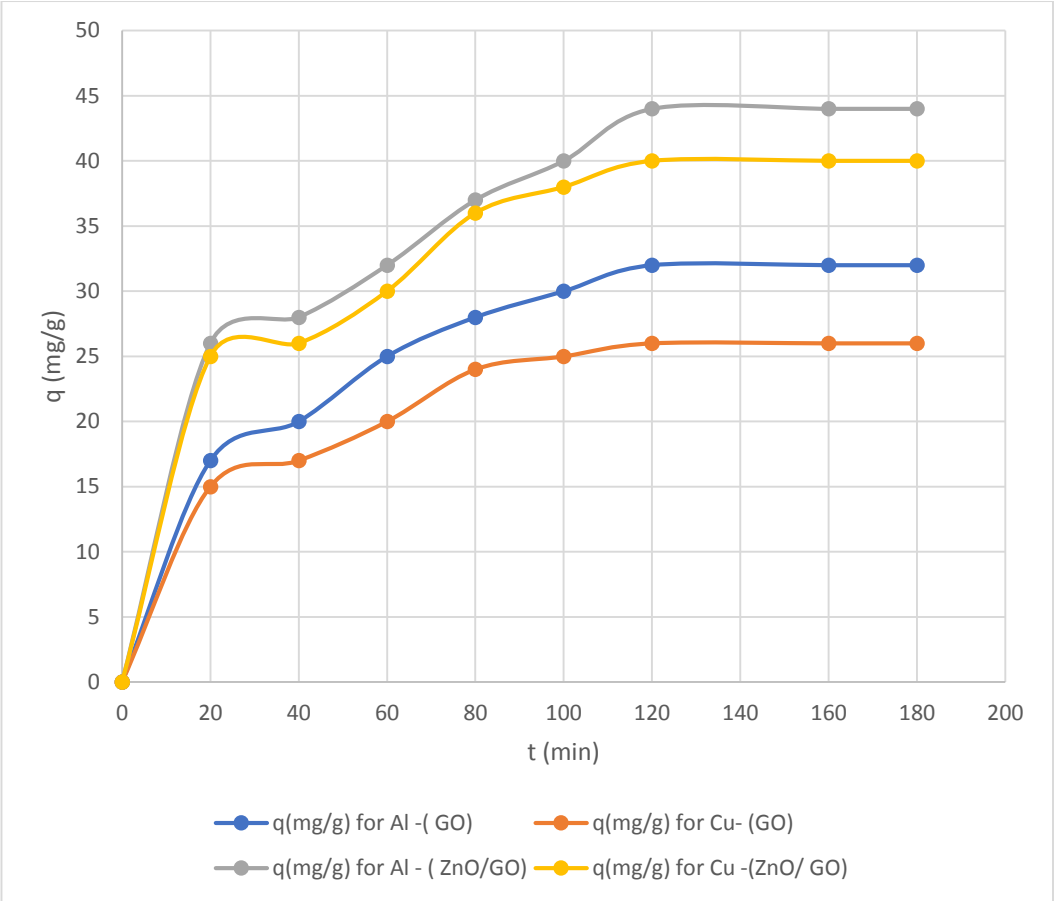

Fig. 6. Kinetic curves for Al and Cu based on the pseudo-second-order model for GO and ZnO/GO nanocomposite.

IV. CONCLUSIONS

In the present study, Al and Cu from a chemical industry wastewater were removed by adsorption using ZnO/GO nanocomposite. The SEM-EDX analysis results showed the presence of ZnO nanoparticles on the GO surface. The pH_{PZC} of GO/ZnO is considerably higher than that of GO and ZnO solely. The removal capacity of Al is higher than Cu.For maximum adsorption yields of Al and Cu the operatinal conditions should be adjusted as follows: Time, pH, nanocomposite concentration, and metal concentration should be 120 min, 6.00, 40 mg/l and 400 mg/l, respectively.

With ZnO/GO nanocomposite other metals in different types of wastewater can be effectively removed. However additional studies should be performed in future to recovery the nanocomomposite and the metals.

REFERENCES

[1]. Goher, M.E.; Hassan, A.M.; Abdel-Moniem, I.A.; Fahmy, A.H.; Abdo, M.H.; El-sayed, S.M. Removal of aluminum, iron and manganese ions from industrial wastes using granular activated carbon and Amberlite IR-120H. Egypt. J. Aquat. Res. 2015, 41, 155–164. [Google Scholar] [CrossRef] [Green Version]

[2]. Bair, D.A.; Mukome, F.N.D.; Popova, I.E.; Ogunyoku, T.A.; Jefferson, A.; Wang, D.; Hafner, S.C.; Young, T.M.; Parikh, S.J. Sorption of Pharmaceuticals, Heavy Metals, and Herbicides to Biochar in the Presence of Biosolids. J. Environ. Qual. 2016, 45, 1998–2006. [Google Scholar] [CrossRef] [PubMed]

[3]. Zhang, W.; Zheng, J.; Zheng, P.; Tsang, D.C.W.; Qiu, R. Sludge-Derived Biochar for Arsenic (III) Immobilization: Effects of Solution Chemistry on Sorption Behavior. J. Environ. Qual. 2015, 44, 1119–1126. [Google Scholar] [CrossRef]

[4]. Liu, N.; Lin, D.; Lu, H.; Xu, Y.; Wu, M.; Luo, J.; Xing, B. Sorption of Lead from Aqueous Solutions by Tea Wastes. J. Environ. Qual. 2009, 38, 2260–2266. [Google Scholar] [CrossRef]

[5]. Rajan, Y.C.; Inbaraj, B.S.; Chen, B.H. In vitro adsorption of aluminum by an edible biopolymer poly (γ-glutamic acid). J. Agric. Food Chem. 2014, 62, 4803–4811. [Google Scholar] [CrossRef]

[6]. Gomaa, H.; Shenashen, M.A.; Yamaguchi, H.; Alamoudi, A.S.; Abdelmottaleb, M.; Cheira, M.F.; Seaf El-Naser, T.A.; El-Safty, S.A. Highly-efficient removal of AsV, Pb^{2+}, Fe^{3+}, and Al^{3+} pollutants from water using hierarchical, microscopic TiO_2 and $TiOF_2$ adsorbents through batch and fixed-bed columnar techniques. J. Clean. Prod. 2018, 182, 910–925. [Google Scholar] [CrossRef]

[7]. Zhang, Y.; Wang, J.; Amrhein, C.; Frankenberger, W.T. Removal of Selenate from Water by Zerovalent Iron. J. Environ. Qual. 2005, 34, 487–495. [Google Scholar] [CrossRef]

[8]. de Meyer, C.M.C.; Rodríguez, J.M.; Carpio, E.A.; García, P.A.; Stengel, C.; Berg, M. Arsenic, manganese and aluminum contamination in groundwater resources of Western Amazonia (Peru). Sci. Total Environ. 2017, 607, 1437–1450. [Google Scholar] [CrossRef] [PubMed]

[9]. Rodríguez, C.; Leiva, E. Enhanced Heavy Metal Removal from Acid Mine Drainage Wastewater Using Double-Oxidized Multiwalled Carbon Nanotubes. Molecules 2019, 25, 111. [Google Scholar]

[10]. Rodríguez, C.; Briano, S.; Leiva, E. Increased Adsorption of Heavy Metal Ions in Multi-Walled Carbon Nanotubes with Improved Dispersion Stability. Molecules 2020, 25, 3106. [Google Scholar]

[11]. Sarma, G.K.; Sen Gupta, S.; Bhattacharyya, K.G. Nanomaterials as versatile adsorbents for heavy metal ions in water: A review. Environ. Sci. Pollut. Res. 2019, 26, 6245–6278. [Google Scholar] [CrossRef] [PubMed]

[12]. Liu, X.; Ma, R.; Wang, X.; Ma, Y.; Yang, Y.; Zhuang, L.; Zhang, S.; Jehan, R.; Chen, J.; Wang, X. Graphene oxide-based materials for efficient removal of heavy metal ions from aqueous solution: A review. Environ. Pollut. 2019, 252, 62–73. [Google Scholar] [CrossRef]

[13]. Selvaraj, M.; Hai, A.; Banat, F.; Haija, M.A. Application and prospects of carbon nanostructured materials in water treatment: A review. J. Water Process Eng. 2020, 33, 100996. [Google Scholar] [CrossRef]

[14]. Kang, Y.G.; Chi Vu, H.; Chang, Y.Y.; Chang, Y.S. Fe (III) adsorption on graphene oxide: A low-cost and simple modification method for persulfate activation. Chem. Eng. J. 2020, 387, 124012. [Google Scholar] [CrossRef]

[15]. Kong, Q.; Preis, S.; Li, L.; Luo, P.; Wei, C.; Li, Z.; Hu, Y.; Wei, C. Relations between metal ion characteristics and adsorption performance of graphene oxide: A comprehensive experimental and theoretical study. Sep. Purif. Technol. 2020, 232, 115956. [Google Scholar] [CrossRef]

[16]. White, R.L.; White, C.M.; Turgut, H.; Massoud, A.; Tian, Z.R. Comparative studies on copper adsorption by graphene oxide and functionalized graphene oxide nanoparticles. J. Taiwan Inst. Chem. Eng. 2018, 85, 18–28. [Google Scholar] [CrossRef]

[17]. Xing, M.; Zhuang, S.; Wang, J. Adsorptive removal of strontium ions from aqueous solution by graphene oxide. Environ. Sci. Pollut. Res. 2019, 26, 29669–29678. [Google Scholar] [CrossRef]

[18]. Standard Methods for water and wastewater examination 2020 Newyork USA

[19]. ang, X.; Liu, Y.; Pang, H.; Yu, S.; Ai, Y.; Ma, X.; Song, G.; Hayat, T.; Alsaedi, A.; Wang, X. Effect of graphene oxide surface modification on the elimination of Co (II) from aqueous solutions. Chem. Eng. J. 2018, 344, 380–390. [Google Scholar] [CrossRef]

[20]. Gohel, V.D.; Rajput, A.; Gahlot, S.; Kulshrestha, V. Removal of Toxic Metal Ions From Potable Water by Graphene Oxide Composites. Macromol. Symp. 2017, 376, 1700050. [Google Scholar] [CrossRef]

[21]. Ranjith, K.S.; Manivel, P.; Rajendrakumar, R.T.; Uyar, T. Multifunctional ZnO nanorod-reduced graphene oxide hybrids nanocomposites for effective water remediation: Effective sunlight driven degradation of organic dyes and rapid heavy metal adsorption. Chem. Eng. J. 2017, 325, 588–600. [Google Scholar] [CrossRef] [Green Version]

[22]. Hadadian, M.; Goharshadi, E.K.; Fard, M.M.; Ahmadzadeh, H. Synergistic effect of graphene nanosheets and zinc oxide nanoparticles for effective adsorption of Ni (II) ions from aqueous solutions. Appl. Phys. A 2018, 124, 239. [Google Scholar] [CrossRef]

[23]. Hua, M.; Zhang, S.; Pan, B.; Zhang, W.; Lv, L.; Zhang, Q. Heavy metal removal from water/wastewater by nanosized metal oxides: A review. J. Hazard. Mater. 2012, 211, 317–331. [Google Scholar] [CrossRef] [PubMed]

[24]. Alswata, A.A.; Ahmad, M.B.; Al-Hada, N.M.; Kamari, H.M.; Hussein, M.Z.; Ibrahim, N.A. Preparation of Zeolite/Zinc Oxide Nanocomposites for toxic metals removal from water. Results Phys. 2017, 7, 723–731. [Google Scholar] [CrossRef]

[25]. Phillips, P.; Bender, J.; Simms, R.; Rodriguez-Eaton, S.; Britt, C. Manganese removal from acid coal-mine drainage by a pond containing green algae and microbial mat. Water Sci. Technol. 1995, 31, 161–170. [Google Scholar] [CrossRef]

[26]. Ambiado, K.; Bustos, C.; Schwarz, A.; Bórquez, R. Membrane technology applied to acid mine drainage from copper mining. Water Sci. Technol. 2017, 75, 705–715. [Google Scholar] [CrossRef]

[27]. Oyarzun, R.; Oyarzún, J.; Lillo, J.; Maturana, H.; Higueras, P. Mineral deposits and Cu-Zn-As dispersion-contamination in stream sediments from the semiarid Coquimbo Region, Chile. Environ. Geol. 2007, 53, 283–294. [Google Scholar] [CrossRef]

[28]. Wu, F.C.; Tseng, R.L.; Huang, S.C.; Juang, R.S. Characteristics of pseudo-second-order kinetic model for liquid-phase adsorption: A mini-review. Chem. Eng. J. 2009, 151, 1–9. [Google Scholar] [CrossRef]